Precision Agriculture, 4, 279–295, 2003
© 2003 Kluwer Academic Publishers. Manufactured in The Netherlands.

Measurement of the Motion of Fertilizer Particles Leaving a Centrifugal Spreader Using a Fast Imaging System

FREDERIC COINTAULT f.cointault@enesad.fr
PHILIPPE SARRAZIN
UMR Cemagref/ENESAD CPAP, Dijon, France

MICHEL PAINDAVOINE paindav@u-bourgogne.fr
LE2I, Université de Bourgogne, Dijon, France

Abstract. Although mechanically simple, centrifugal spreaders used for mineral fertilization involve complex physics that cannot be fully characterized at the present time. We are developing sensors to evaluate the spatial distribution of the fertilizer on the ground based on the measurement of initial flight conditions of fertilizer granules after their ejection by the spreading disk. The techniques developed are based on the analysis of images of the area around the disk showing the granule ejection. A high resolution – low cost imaging system for the analysis of high speed particle projection developed for this specific purpose is presented in this paper. The system, based on a camera and a sequence of flashes, is used to characterize the centrifugal spreading of fertilizer particles ejected at speeds of approximately 30 $m\,s^{-1}$. It automatically computes the direction of ejection and velocity of each granule observed in the image. Multi-exposure images collected with the camera installed perpendicular to the output flow of granules are analyzed to estimate the trajectories of the fertilizer granules, using different motion estimation methods.

Keywords: centrifugal spreading, particle ejection, image analysis, motion estimation, trajectories, multi-exposure images

Introduction

Precision agriculture relies on the availability of precision equipment. Although most manufacturers of granular fertilizer spreaders are adapting their products to variable rate fertilization, very few products can actually provide sufficiently accurate control of the rate of application of fertilizer (variation coefficient (CV) often greater than 10%, which corresponds to bad fertilization). A lot of research and development work has been focused on geographical information systems (GIS), positioning techniques (GPS), remote sensing for soil and crop characterization, and adaptation of agricultural equipment to the accurate control of their operation. The low cost, simplicity and general robustness of centrifugal spreaders have made this type of fertilization equipment widespread in Europe (90% of the market for mineral fertilizer spreaders). However, it actually involves complex physics that, at the present time, cannot be fully characterized during operation. Most attempts to modify centrifugal techniques for variable rate fertilization have been based on controlling a single parameter: the flow rate of granules. Various designs of sensors have been proposed, either based on measurement of the

variation of mass of the fertilizer left in the hopper or by measurement of the power absorbed by the spinning disk during spreading (Cointault *et al*., 2000). The current local fertilization rate on the ground is the result of both the instantaneous fertilizer flow and the instantaneous spatial distribution provided by the spreader. Accurate control of the local fertilization rate requires control of these two parameters. None of the commercial spreaders available to date allows evaluation of both parameters. We are studying techniques capable of fully characterizing the instantaneous distribution of fertilizer on the ground. Direct measurement of the spatial distribution on the ground is practically impossible. Previous studies (Colin, 1997; Hofstee, 1994; Olieslagers, 1997) have shown that the spatial distribution on the ground can be accurately estimated by calculating the ballistics of the particles from their initial conditions of flight (velocity, direction), their properties and geometrical parameters (topography, height and tilt of the disks, . . .). Our approach is focused on the characterization of the initial conditions of flight of the granules in the vicinity of the disk. The quality of distribution of the granules on the ground is directly dependent upon these ejection distributions, which vary depending upon numerous parameters such as the nature of the fertilizer, the blades and feeding system geometries, the rotation speed and the mass flow. Generally, misadjustment of centrifugal distributors are often responsible for uneven fertilization which is harmful to the environment and affects crop. The initial aim of the research program was to develop high speed imaging techniques. The work described here led to a system for characterizing the centrifugal spreading in a laboratory or a testing facility. The system will be applied as a reference tool for developing simpler image based sensors that could be practically applied to the control of spreaders in the field, or as a system for testing the quality of conventional spreading systems under various conditions. The initial conditions of flight are then used as input data in ballistic models to obtain the fertilizer distribution on the ground. In response to the output information from such a system, different control parameters of the disk can be adjusted such as rotation speed, mass flow, feed point of the granules on the disk and height between the disk and the hopper.

The paper presents the design of imaging techniques intended to accurately characterize the spatial distribution of centrifugal spreaders during their operation. We hope to determine the ejection velocity of the granules with an error lower than 1%, in comparison with real velocity. The experimental setup designed to test the techniques and the fast imaging acquisition system are presented in the second section. Images collected with this system and analyzed with motion estimation methods are then presented. Finally, possible developments of our system are discussed.

Experimental setup and imaging technique

General description of the prototype

Figure 1 presents the rig constructed for testing the techniques. It was composed of three independent frames.

On one frame was mounted the spreading system composed of a flat disk fitted with two radial blades. The disk was installed with a vertical axis on a double ball bearing

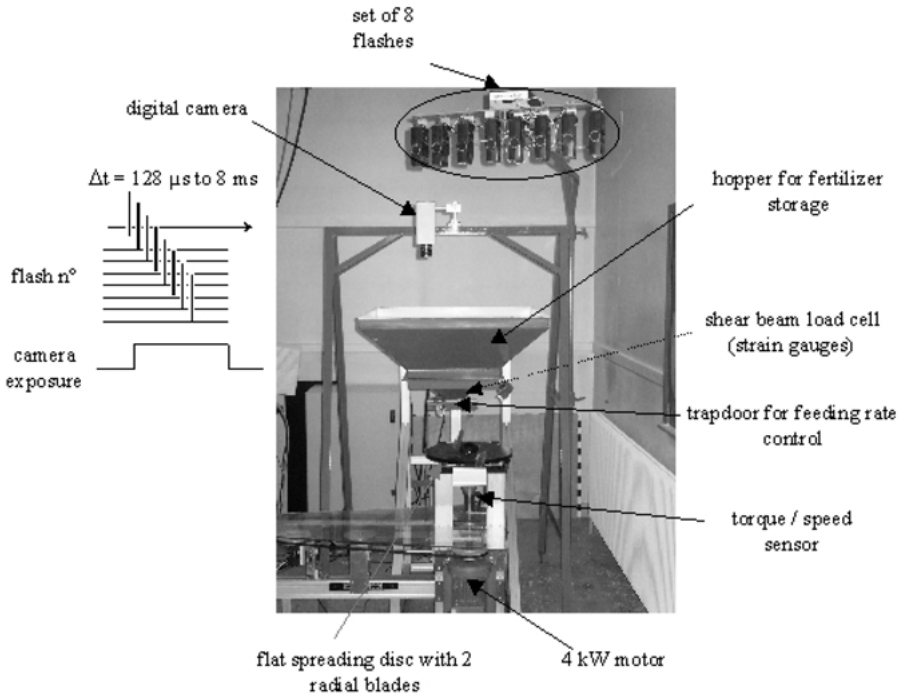

Figure 1. Testing rig with imaging system installed.

assembly. The disk was driven by a 4 kW asynchronous AC motor. A programmable power supply provided speed control. The power was transmitted to the disk though a DR-20 (Scaime SAS—ZI Juvigny, BP 501, 74105 Annemasse Cedex, France) rotary torque and speed sensor. This sensor has been used for developing a fertilizer mass flow measurement technique described by Cointault *et al*. (2000).

A separate frame held a hopper that had a capacity of approximately 60 kg of fertilizer. The flow of fertilizer was controlled by a horizontal sliding door at the bottom of the hopper. This trap door was electrically activated and fitted with a position sensor. The hopper was mounted on a AB 100F (Scaime SAS—ZI Juvigny, BP 501, 74105 Annemasse Cedex, France) single point load cell to measure the weight of fertilizer and calculate the mass flow during operation. The relative position of the hopper and spreading system frames could be adjusted to provide the appropriate feeding point of fertilizer granules onto the disk.

A third frame held the imaging system, composed of a high resolution black and white camera, placed vertically above the granule output flow at a distance of 890 mm, and a custom made flash system. Two arms allowed independent adjustment of the positions of the camera and flash unit. The flashes were placed 1500 mm above the plane of the disk and their orientation optimized to give the best lighting of granules in flight.

The major difference between the experimental rig and a commercial distributor is that only one spreading disk is used.

Characteristics of fertilizer output flow and sensors

The granules were ejected by the rotating disk at speeds of approximately 30 $m\,s^{-1}$. High speed imaging techniques were chosen for characterizing this high speed ejection.

Initial tests were performed using a high speed camera HSV 500 NAC (Kodak-Pathé France, 26 rue Villiot, 75594 Paris Cédex 12) providing a frame rate of 250 frames per second (fps) or 500 fps. At a frame rate of 500 fps, eight images of a granule were shown to be sufficient to characterize the particle motion using motion estimation methods such as Gabor filters (Heeger, 1987; Pellerin *et al*., 1996) and Markov Random Fields (MRFs) (Horn and Schunck, 1981; Kardouchi *et al*., 1997). However, the 350×262 pixels image format could not provide the resolution required to cover the field of view of approximately 1 m $\times$ 1 m necessary to image the whole angular range of projection.

There are very few cameras combining high resolution and high frame rate and they are very expensive. They were not suitable for this application. An alternative technique has been developed combining a high resolution slow speed camera in conjunction with a strobe system.

The camera used in the experiments was a Kodak MEGAPLUS ES 1.0/MV low frame rate, high resolution digital CCD camera. It operates in single channel mode and allows capture of up to 15 images per second with a resolution of over one million-pixel with an 8-bit dynamic range. In order to cover the desired field of view—that is a 1 m^2 area—with low radial distortion, we chose a 8.5 mm focal length COSMICAR C815B lens, which had an angle of view of 56°.

No strobe system combining the speed and lighting power required for this application was commercially available, so a special flashing unit was built using a series of photographic flash unit triggered one after the other over a single camera exposure. The number of flashes determined the maximum number of positions that could be recorded on each image. Motion estimation methods based on Gabor filters require at least seven positions, so a set of eight flash units was built.

Eight VIVITAR 2800 auto-thyristor flash units were modified to give very short flash duration in order to prevent blur due to high speed motion of the granules. Flash duration was reduced to approximately 30 μs by exposing the light sensor used in the automatic power adjustment circuit to the direct flash light. The flashes were triggered in sequence by a digital controller which also triggered the camera before the first flash operated. The controller allowed adjustment of the delay between two successive flashes from 128 μs to 16 ms and synchronized the flash sequence with the disk so that the first flash was always triggered at a given angular position of a blade. The recycling time was programmed in the controller and was adjustable from 0.5 to 5 s. A 1 s recycling time was shown to be the best compromise to allow full recharge of each flash unit capacitor.

Image acquisition setup

Multi-exposure imaging. The scheme in Figure 2 summarizes the principle of the multi-exposure imaging technique also called chronophotography.

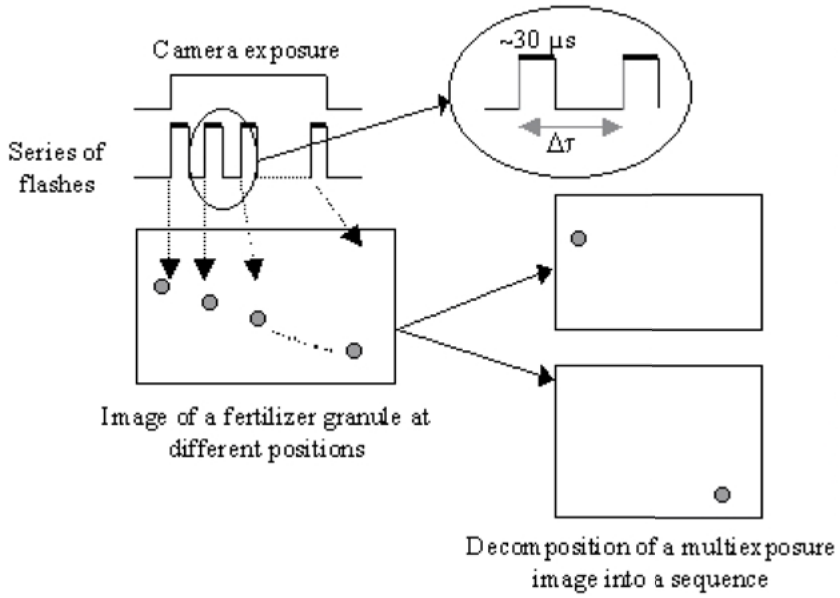

Figure 2. Scheme showing the principle of the multi-exposure system.

The technique was based on the recording of an image superimposing several successive positions of a fertilizer granule. When N flashes were triggered during a single camera exposure, the resulting image showed N successive positions of the fertilizer granule. The delay Δt between successive flashes was accurately controlled so that the particle velocities could be calculated from the distance between the successive positions in the image. When Δt of an image was high enough so that no overlapping of successive positions occured, the image could be decomposed into a sequence of N images, simulating the output of a conventional high speed camera.

Image calibration

Distortions due to the lens have been observed on images collected with the camera. In order to avoid errors in the velocity analyses, a calibration method developed by Heikkilä and Silvèn (1997) has been used. This method uses a checkerboard photographed in different positions. An algorithm determines automatically the intersection points of all the black and white squares and extracts the intrinsic and extrinsic parameters of the camera used to rectify the distorted images.

Figure 3 shows, at the upper left side, a raw checkerboard image collected with the system described earlier and, at the upper right side, the same image after rectification of the radial distortion. The distortion appears clearly in the corners of the image and decreases from the side to the center. The third image presents the superimposition of the two previous images to clearly show the distortion.

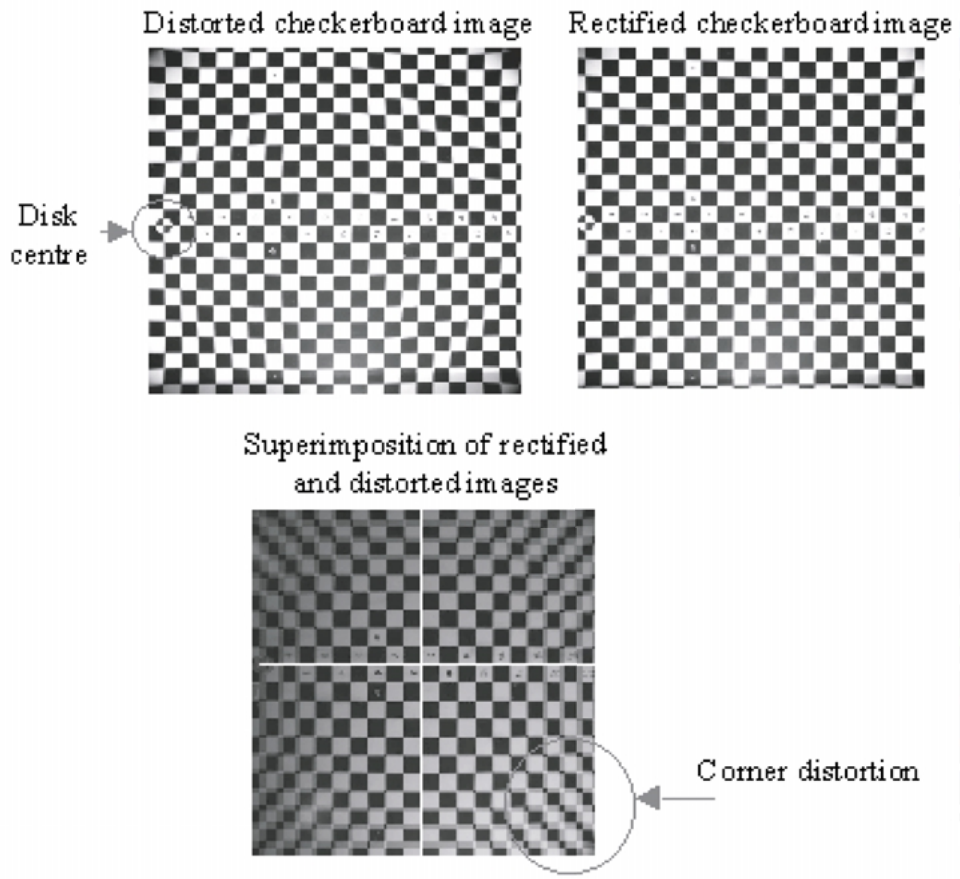

Figure 3. Image calibration using a checkerboard.

In addition to the rectification of the image distortion, the checkerboard was used to spatially calibrate the image acquisition setup. The checkerboard was mounted very precisely on the frame holding the spreading disk. It showed the centre of the disk and provided an x and y scale, each black or white cell measuring exactly 50 mm $\times$ 50 mm. This calibration was an essential step in the image pre-processing because the disk center co-ordinates and the blade radius in pixels were required for modeling the trajectories. The image rectification indicated that the distortion induced an error in an image of approximately 20 pixels on the X axis and 2 pixels on the Y axis.

Analysis methods and results

Imaging techniques

Images collected with this system have to be analyzed with motion estimation methods in order to determine the motion vectors of the projection. Image processing techniques

adapted for this purpose have been described in numerous publications such as Beauchemin and Barron (1995) or Orkisz and Clarysse (1996). Briefly, the techniques can be summarized as follows:

Technique based on a single image. A model of the instantaneous spatial distribution of granules—that is a model of the shape of a trajectory of a fertilizer granule observed at a given time—is applied on a single image of a sequence obtained as presented above. This step allows the average characteristics of the motion of the particles to be determined. This simple technique can approximate the actual motion field but does not take into account the variation of ejection velocities. Although it only provides approximate data, it has been shown to be very useful for analyzing motion prior to more complex refinements.

Techniques based on two successive images. Intercorrelation (cross-correlation) methods, widely used in motion estimation, only provide global parameters. Tests have shown slightly better results than the first technique described above.

The Markov Random Fields (MRFs) technique on the other hand refines the motion vector locally. It has shown very satisfactory results when modified so that the motion field is first initiated with the result of a prior analysis performed on a single image as described above (see Section titled Refined motion analysis for more explanations).

Technique based on sequence. The Gabor filters method works in the frequency domain and requires the use of a sequence of at least seven images. 2D Gabor filters are used in image analysis and are defined as the modulation of a bidimensionnal gaussian function by a plane wave. The expression below is the mathematical expression of this modulation (where f_{x_0} and f_{t_0}, are respectively the spatial and temporal central frequencies, σ_x and σ_t, respectively the spatial and temporal bandwidth of the filter, x and t the two dimensions of the filter):

$$g(x,t) = \frac{1}{\sigma_x \sigma_t (\sqrt{2\pi})^2} \exp\left\{ -\left[\frac{x^2}{2\sigma_x^2} + \frac{t^2}{2\sigma_t^2} \right] \right\} \times \left\{ \begin{matrix} \cos(2\pi f_{x_0} x + 2\pi f_{t_0} t) \\ j \sin(2\pi f_{x_0} x + 2\pi f_{t_0} t) \end{matrix} \right\} \quad (1)$$

If the motion of a small area in the image can be approximated by a translation in the image plane, the speed of this same area can be calculated in the Fourier domain, by finding the plane in which all the power is. To extract optical flow, small spatiotemporal windows can be taken, outside the image sequence, in order to set a plane on each power spectrum. But for an oriented pattern, little information in the image sequence is available to exactly define the right direction of the motion. In the spatiotemporal domain, power spectrum of this image is restricted to a line and the different planes containing this line correspond to the possible speeds. The normal flow, defined as the motion component in the direction of the image gradient, is the slope of this line. Spatiotemporal bandpass filters are not selective to a particular speed but are adjusted on spatiotemporal frequencies and do not allow alone speed estimation. To calculate the speeds, a whole set of filters is necessary, each filter being adjusted to a different frequency. Its adaptation to motion analysis of fertilizer granules and its performance are currently being investigated, but no results are available for the moment.

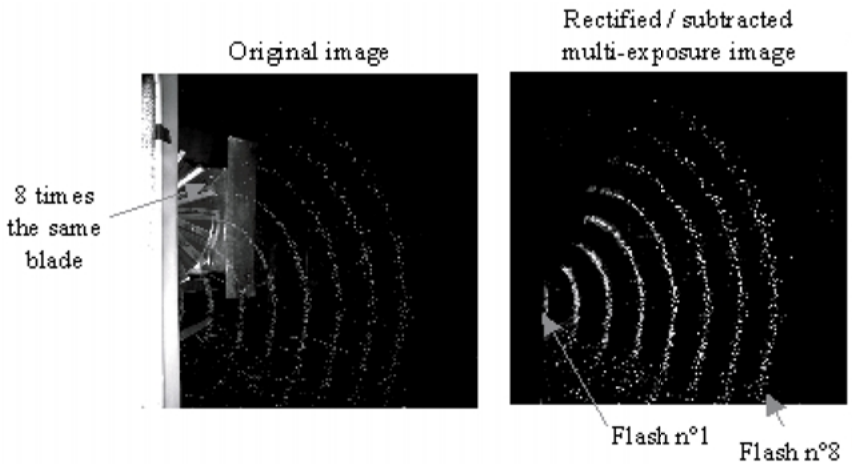

Figure 4. Image collected with the multi-exposure system.

Multi-exposure images

Figure 4 shows an example of a multi-exposure image obtained with the following conditions: fertilizer NPK 17–17–17 (Nitrogen, Phosphate, Potassium, granulo-metric spreading of 1.81 mm, density of 1.056, mean diameter of 3.67 mm, mean discharge of 0.1635 kg s^{-1}), delay between flashes = 4.096 ms, mass flow = 0.4 kg s^{-1}, 275 mm radius blades, rotation speed = 800 rpm. In this case, the field covered by the granules was approximately 1 m^2. Figure 4 (left) shows the raw image. A background image was recorded prior to any test, in the same operating conditions but without any fertilizer flow. The background image was subtracted from a raw image. The resulting image was then corrected for radial distortions. The result of this processing is shown in Figure 4 (right).

When the delay is adjusted so that two successive positions do not overlap (as in Figure 4), the multi-exposure image can be decomposed into a sequence of eight images as presented in Figure 5.

After this decomposition, we used different motion estimation methods to obtain the granule trajectories. These methods are briefly explained in the next paragraphs and results of motion estimation are given too.

Initial image analysis. A theoretical model of granule distribution was fitted to the image to extract mean parameters of the ejection velocity. The observed distribution of granules at time t shows a crescent shape. Figure 6 presents a scheme of a twin blade spreading disc at two different times: O, is the center of the disc, r, the blade radius, M, the ejection point of a given granule at time t_1, P, the location of the same particle at time t_2, Ω, the ejection angle and ω, the angular velocity. The tangential speed of the granule at the ejection is $V_t = r\omega$. Patterson and Reece (1962) have shown that, at the ejection and with a flat disk and radial blade configuration, the radial speed is

$$V_r = ar\omega \tag{2}$$

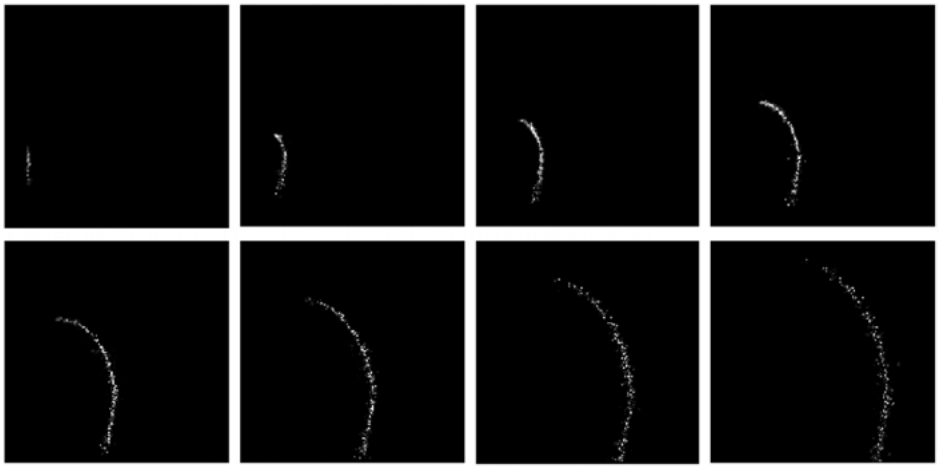

Figure 5. Decomposition of a multi-exposure image into a sequence of 8 images.

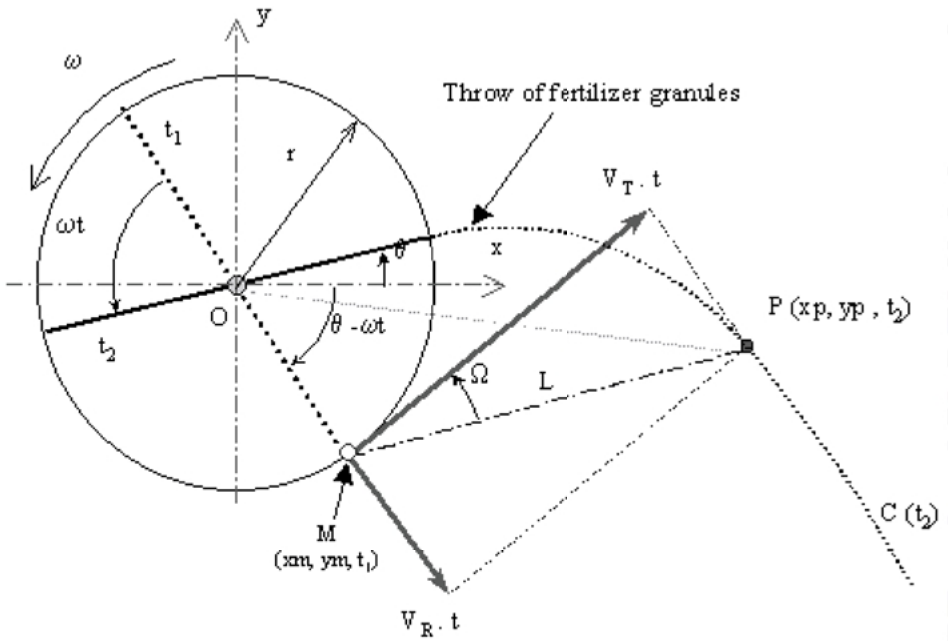

Figure 6. Scheme of a twin-blade disc at two different times t_1 and t_2.

where a is a parameter dependent on the friction coefficient μ of the granule on the blade:

$$a = \sqrt{(\mu^2 + 1)} - \mu \tag{3}$$

in its simplified expression. In a simple model that does not take into account the aerodynamic drag of the particle during the flight, one can assume that the velocity of the

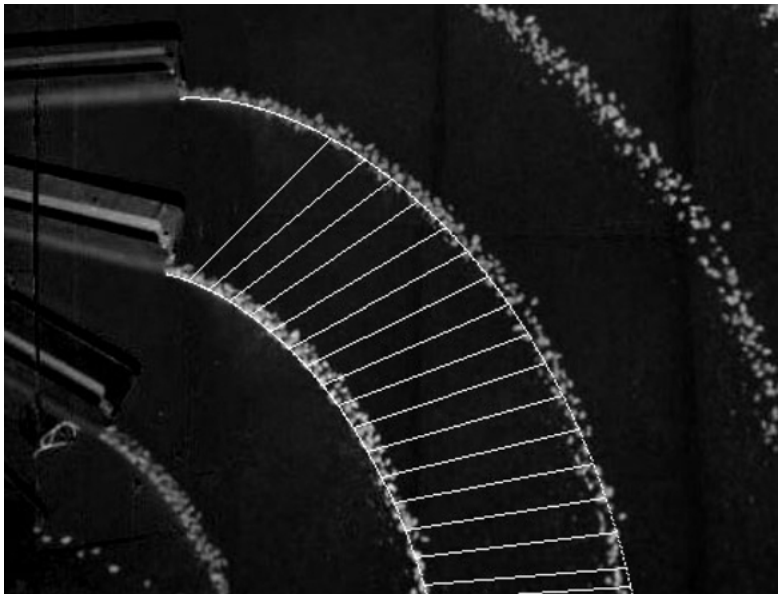

Figure 7. Example of calculation of motion vectors.

particle remains constant in direction and magnitude in the vicinity of the disk. As such, $\overrightarrow{MP}$ gives the direction and magnitude of the granule velocity.

At time $t_1(t_1 = 0)$, a particle is ejected from the blade at tangential speed V_t and radial speed V_r whereas at time $t_2(t_2 = t)$, the same particle has flown to P and the blade has rotated an angle ωt. The theoretical velocities for each possible position of the granules in the image are given by:

$$\begin{aligned} V_x &= ((xp - xm)r\omega\sqrt{1 + a^2})/L \\ V_y &= ((yp - ym)r\omega\sqrt{1 + a^2})/L \end{aligned} \tag{4}$$

$$\text{with} \quad L = \sqrt{(xp - xm)^2 + (yp - ym)^2} \tag{5}$$

The parameter a can be calculated from the multi-exposure images, which contain sufficient information to infer this parameter, using different methods.

The first method is to determine the ejection angle Ω and then with Eq. (3) to recover a. This method is not very accurate because of the great uncertainty about the calculation of Ω. The second consists of using the values of the dynamic friction coefficient μ given by different authors such as Colin (1997) or Adjroudi (1993), and then to calculate the corresponding parameter a. However, there is no consistency in the reported values of a. Depending on the measurement system used, the values of this parameter vary significantly. This solution has been eliminated.

For the third method, we make varying the parameter a between 0 and 1, and for each value, we have a theoretical projection of a given throw. Then we sum, for each

projection, the pixel values and we obtain then a gaussian. When the sum is maximum, we consider that we are in the middle of the throw and then we have the a parameter. Because we used eight flashes, eight values of a were found and we can then deduce the vector $\bar{a}$. This technique needs however to have a constant illumination on the whole crescent, which is not very easy to obtain. Then, a fourth method consists of taking a crescent and varying a. The following crescent is then reconstructed for each value of a. Then we calculate, for each reconstructed crescent the gap between the intensities of the real and reconstructed crescents: it is assumed that the lowest intensity indicates the optimum value of a. This last method has been used when comparing the different methods.

After the calculation of a, an approximated motion field is computed using (4). Figure 7 presents a superimposition (rotation speed = 700 rpm) of a real image and a few motion vectors calculated between throws number 4 and 5 with the modeling.

In the previous case, the distance between two successive throws was of 12 ± 2 pixels. The difference between observed and calculated motion was about 3–5 pixels which gives an error between 2.4% and 4%. This error is within the range of MRFs method that can then be used to refine the motion field of each individual granule. This simple technique can approximate the actual motion field but does not take into account the variability of ejection velocities. Even if it only provides approximate data, it has been shown to be very useful as an initial motion analysis prior to more complex refinements.

Refined motion analysis: Adaptation of MRFs. The MRFs method is based on a probabilistic method and on the determination of the optical flow. The main hypothesis is the invariance of luminosity of a pixel between two successive images. The markovian approach provides, moreover, a strong and global mathematical frame allowing to define local nonlinear interactions between the pixels, when taking into account the interactions between the pixels and other information. The local nature is expressed by the definition of a neighbourhood for each pixel of the image.

The basic idea is then to extract primitives or labels (that is a displacement vectors field) from observations (typically two successive images of the same sequence).

The formulation of this problem consists of the minimization of a function (called energy function) including several local constraints. The construction of this function relys on a global knowledge of the problem to be treated and on *a priori* knowledge of primitives. This method needs the use of an initial displacement vectors field, generally equal to zero because the displacements are not very important in magnitude. In our case, the displacement of a granule between two images is approximately 75 pixels which is not in the range of 4–6 pixels required by the MRF technique and obtained by some previous results given by other papers (Kardouchi *et al*., 1997).

In order to reduce the size of the displacements, so as to use the MRFs method, different methods can be used. First of all, we can implement the multi-resolution method: this method consists to create different resolution levels for two successive images, that is we define a pyramid of these images. The initial sizes of the images are divided by 2 (using a low-pass filter (smoothing of the energy function)), in the two directions, to obtain the same images with lower resolution. We can define as many levels as we want and at the final lowest resolution, only the largest displacements of the initial resolution are available. We finally obtain a pyramid for the twice images, then we estimate the

motion at the lowest level, with an initialization vectors field equal to zero. The result is then used as the initialization vectors field for the next level. The process starts again until the original level is reached. This method allows evaluation of large displacements, but for large objects or objects which overlap from one image to the next (Graffigne *et al*., 1995; Kardouchi *et al*., 1997). In our case, the granules have a size of 5 pixels diameter in an image size of one million pixels. The smoothing of the image (when using the low-pass filter) leads to the elimination of the motion when using the multi-resolution technique.

Another method reduces the flash delay in order to reduce the displacement between two successive images. But to be in the range allowed by the MRF method, we have to set a 256 μs flash delay which does not allow decomposition of the multi-exposure in a sequence of images, because of the overlap between the granule throws.

The last method was then to use a technique which can approach the real displacement vectors field and after to use this field as an initialization field for the MRF method.

That is why the motion vector field calculated as described in the previous section is used as an initialization field for the MRF motion field refinement. The modeling assumes that all the vectors have the same magnitude but that is not true because of the interactions between granules and their characteristics. Initial results have confirmed that the MRF motion analysis leads to a much more accurate motion field as shown in Figure 8 (test carried out with KCl (Potassium chloride:granulometric spreading of 2.10 mm, density of 1.013, mean diameter of 3.60 mm, mean discharge of 0.1428 $kg\,s^{-1}$) and short blades (225 mm), rotation speed of 600 rpm, trap aperture of 25 mm (i.e. a mass flow of 0.56 $kg\,s^{-1}$)). Each block of three figures agrees with the same part of the original image. The difference between the two blocks is that, in the second block, crescent 6 is recovered from crescent 8 whereas, in the first block, crescent 5 is recovered from crescent 6.

Figure 8(b)–(e) represent the superimposition between the original images (8(a)–(d) in black pixels) and the reconstituted image with initialization vectors (in white pixels). A spreading out of the crescent due to the gap between the original positions and the modeled positions of the pixels does not allow the real image to be recovered exactly. Figure 8(c)–(f) represent the superimposition between the original images (black pixels) and the corrected image with ''markov'' vectors (white pixels).

The last superimpositions do not show any notable differences between the original and corrected positions of the pixels. The real positions of the granules are reconstituted much more accurately with the Markov vectors. This can be seen in Figure 8(e) where the initialization vectors do not allow the real image to be obtained. Consequently, the markov vectors are very small in comparison with the main trajectory velocities. All these results justify the use of the MRF method to correct the direction and the magnitude of the granule velocities. Further improvements of the MRF analysis are being tested at the present time and will allow calculation of the distribution of velocity and direction of ejection. Each multi-exposure image contains eight times the same throw. After the decomposition of this image, we note by $C2, \ldots, C8$ the different crescents, where C2 is the first crescent of the ejection and C8 the last.

Table 1 gives instantaneous speeds obtained for the ammonium nitrate fertilizer (granulometric spreading of 1.89 mm, density of 0.943, mean diameter of 3.53 mm, mean discharge of 0.1567 $kg\,s^{-1}$), for two different granules in the same throw. These granules

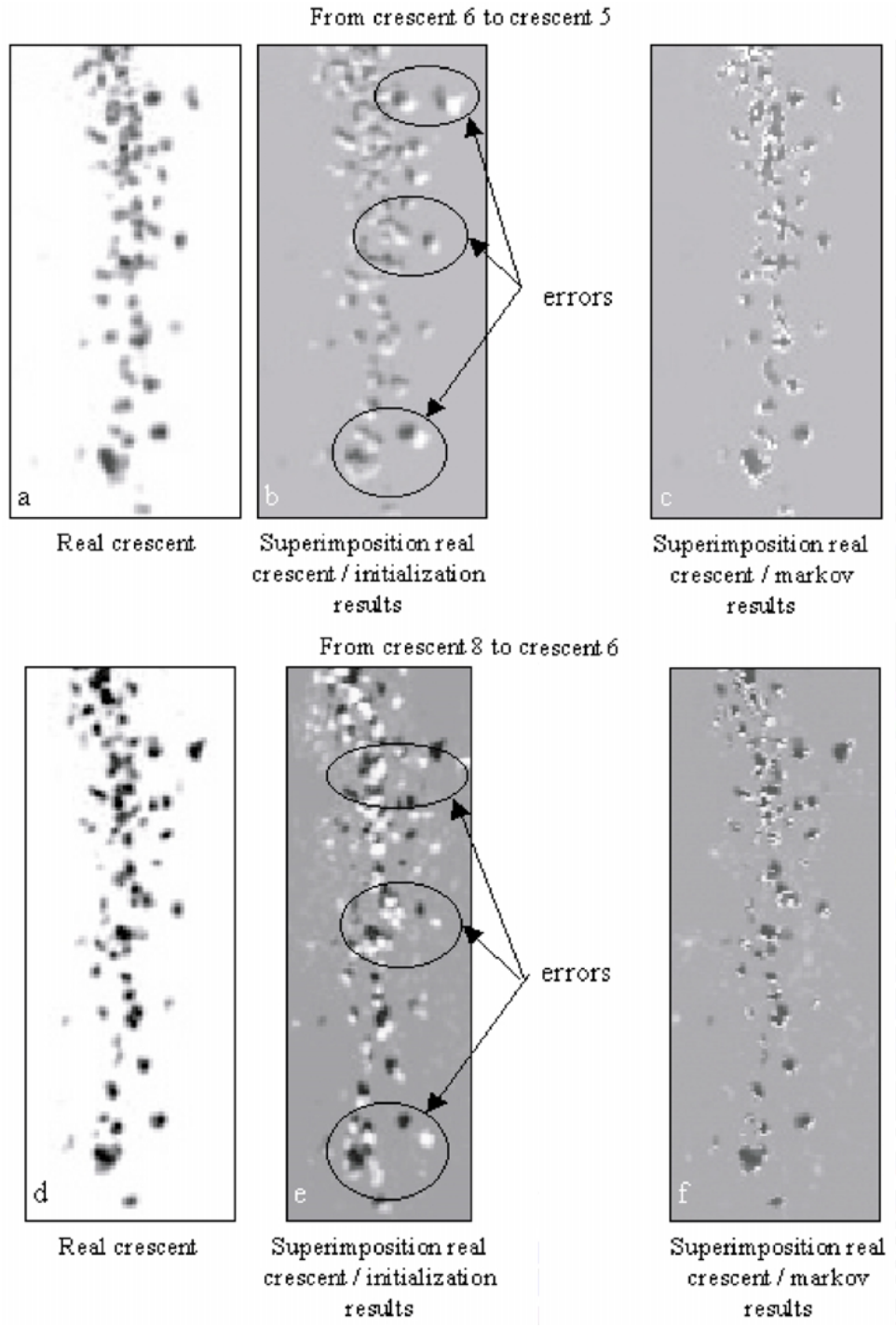

Figure 8. Results for the motion estimation with the MRF method.

Table 1. Comparisons between different speeds for the ammonium nitrate

Speeds (m s^{-1}) flash delay 2.048 ms	$\omega = 800$ rpm Blades (325 mm) Aperture = 25 mm	$\omega = 800$ rpm Blades (325 mm) Aperture = 25 mm
Model speed (V_i)	33.54	33.43
Markov speed (V_m)	34.04	33.92
Real speed (V_r)	34.02	33.9
$(V_m - V_r)/V_r$	0.06%	0.06%
$(V_i - V_r)/V_r$	−1.40%	−1.39%

Table 2. Standard deviation (Std. Dev.) and errors obtained for the ammonium fertilizer in the previous conditions

Average real speed $\overline{V_r} = 33.97$ m s^{-1}	Std. Dev. (m s^{-1})	Min. error/$\overline{V_r}$	Max. error/$\overline{V_r}$
Model speed (V_i)	0.239	0.43 m s^{-1} (1.26%)	0.54 m s^{-1} (1.61%)
Markov speed (V_m)	0.049	0.00 m s^{-1} (0.00%)	0.07 m s^{-1} (0.21%)

Table 3. Comparisons between different speeds for the NPK 17–17–17

Average speeds (m s^{-1}) flash delay 4.096 ms	$\omega = 800$ rpm Blades (325 mm) Aperture = 25 mm	$\omega = 800$ rpm Blades (275 mm) Aperture = 20 mm
Model speed (V_i)	32.61	26.19
Markov speed (V_m)	32.59	26.63
Real speed (V_r)	32.54	26.63
$(V_m - V_r)/V_r$	0.15%	0.00%
$(V_i - V_r)/V_r$	0.22%	− 1.65%

Table 4. Standard deviation (Std. Dev.) and errors obtained for the NPK fertilizer for the average blades

Average real speed $\overline{V_r} = 26.44$ m s^{-1}	Std. Dev. (m s^{-1})	Min. error/$\overline{V_r}$	Max. error/$\overline{V_r}$
Model speed (V_i)	0.236	0.04 m s^{-1} (0.15%)	0.52 m s^{-1} (2.00%)
Markov speed (V_m)	0.111	0.00 m s^{-1} (0.00%)	0.25 m s^{-1} (0.95%)

have been randomly chosen. The corresponding standard deviation and minimum and maximum errors for this test are given in Table 2. Table 3 gives average speeds (for one random granule) obtained for the NPK (Nitrogen, Phosphate, Potassium) 17–17–17 fertilizer (see Section titled multi-exposure images for the fertilizer characteristics).

Table 4 presents the standard deviation and minimum and maximum errors for this test. The variation of the aperture allows modification of the mass flow. The real speed was calculated manually between two successive images: we first measure the distance,

in pixels, between the positions N and $N+1$ of the same granule. The uncertainty for the distance calculation is about 0.20 pixels. Knowing the flash delay and the ratio pixels/mm, we deduce the real speed. The ratio depends on the precision of the calibration: it is given with a precision of ± 0.0015. When taking into account the different uncertainties, the real speed is given at $\pm 0.28\ \mathrm{m\,s^{-1}}$.

In Table 1, the flash delay of 2.048 ms involved a distance between two successive throws of 76 ± 1 pixels. In this case, the errors detected were 1–3 pixels, which corresponds to errors of 1.3–4%, with the modeling method. For the same fertilizer as in Figure 7, the errors are smaller, because of the shorter distance.

As shown in Tables 1–4, the markov results are better than the results obtained with other methods. The nature of a centrifugal spreader does not allow very accurate transverse distribution on the ground. Therefore, the errors obtained with our modeling technique may be considered as negligible in the field. However, for the laboratory experiments, we wish to have as accurate results as possible in order to evaluate different motion estimation methods. Even though we could not evaluate precisely the effects of drag and lift on the fertilizer granules, we can assume that these effects have an undesirable influence on the projection and then the distribution on the ground. It would be interesting to measure the velocity of the air at the ejection in order to take into account this parameter in our model. However, in our project, we have deliberately limited the study to the determination of the initial conditions of flight of the granules, up to 1.5 m after the ejection. In this case, the effects of drag and lift may be negligible.

The use of the combination of two methods, that is the modeling of the trajectories and the markov random field method, gives results that are very close to the values of the real speed. They may then be then used as initial conditions for ballistic models.

Future developments

In order to avoid the cost problem, simpler imaging techniques (called mono-exposure techniques) derived from the one described above are currently being investigated. Based on simpler hardware and faster processing algorithms, they should provide average values of basic parameters of spreading such as the average velocity and the angular distribution of the flow of particle, for a cost of approximately 1500 euros, which corresponds to the basic cost for implementing a system on a spreader. A spreader fitted with this type of image sensor coupled to a fertilizer flow sensor being developed in parallel in our laboratory (Patent No 0109749 2001), should enable real time control of the spatial distribution of fertilizer required for accurate variable rate fertilization. This can be realized by calculating the ballistics of the particles. According to Colin (1997), the trajectories of the granules are rectilinear, with a flat spinning disk, up to 2 m after the ejection. In our case, the vertical discharge angle is negligible, because the field of view is only approximately 1 m^2. The level of performance improvement to be expected cannot be estimated at present because the study was limited to the determination of the initial conditions of flight of the granules in the vicinity of the spreading disk.

However, we are trying to adapt the technique described with a concave disk and different kinds of blade. Always, according to Colin (1997), when using concave disks, the vertical angle for the granules is small up to 1 m after the granule ejection. It is

reasonable to neglect the possible small initial vertical velocity component for the trajectories, up to 1 m after the ejection. To confirm this, a second camera will be used to monitor the vertical movement of the granules at the output.

Airflow conditions

We intend to study the airflow conditions close to the discharge point of the granules. Our vision system cannot provide information about such conditions at present. The system takes into account all the granule interactions on the blade and is then much closer to reality. Indeed, the existing models use theoretical equations which consider a single particle with no interactions with others or with the blades. With our imaging technique, we are evaluating the movement of the granules on the blades, theoretically and experimentally, but at present we have only images taken with our vision system.

Other applications

The field of application for the technique is much broader than the specific characterization for which it was designed. The system is a cost-effective substitute for many motion estimation systems based on high speed videography. The application is however limited to single objects or organized groups of objects, that move fast enough so that successive positions do not overlap. Studying short displacements that involve overlaps is possible if one uses a color camera and a set of three (or multiple of three) flashes fitted with red, green and blue filters, respectively. In such a system, each color component in an RGB image would correspond to a position of the object. This setup has been investigated for our system using a color CCD digital camera and color filters on the flash. Although most filters strongly absorb the light emitted by the flashes, the technique has been shown to be usable when there is risk of overlap.

Conclusion

The spreading characterization technique described in this paper allows full characterization of the ejection of fertilizer granules. The sequence of images obtained with this technique is similar to the output of a high speed camera, but with the advantage of better spatial resolution and signal to noise ratio, for only a fraction of the cost of a high speed camera. When combined with a ballistic model, it will allow computation of the spatial distribution of granules on the ground. The information provided by this imaging technique involves technological complicity but the computation time is short enough to allow real time control of a spreader.

The imaging technique described here may be used to characterize centrifugal spreader performance in a testing facility and could serve as a research and development tool for studying and designing centrifugal spreaders and applied sensors. The cost of the system is currently too high to use on a centrifugal spreader in the field; a commercial spreader costs between 7500 and 12,000 euros and our proposed system costs about 12 000 euros.

References

Adjroudi, R. 1993. Comportement d'un flux de particules solides hétérogènes sous l'action d'un lanceur rotatif (Behavior of heterogeneous solid particle flow under the effect of a rotary launcher). Ph.D. Thesis (Institut National Agronomique Paris-Grignon, France).

Beauchemin, S. S. and Barron, J. L. 1995. The computation of optical flow. ACM Computing Surveys **27**(3), 433–467.

Cointault, F., Sarrazin, P., Rousselet, M. and Paindavoine, M. 2000. Modulation of the centrifugal spreading of the granules fertilizers: Flow measure and determination of the particles trajectories by imagery. In: *Colloque AP2000: Actes du colloque Agriculture de Précision*, edited by Educagri editions (Dijon, France), pp. 321–335.

Colin, A. 1997. Etude du procédé d'épandage centrifuge d'engrais minéraux (Study of the centrifugal spreading process of fertilizer). Ph.D. Thesis (Université Technologique de Compiègne, France).

Graffigne, C., Preteux, F., Sigelle, M., Zérubia, J. Pérez, P. and Heitz, F. 1995. Hierarchical markov random field models applied to image analysis: A review. In: *Image and Signal Processing Proceedings, SPIE Conference No 2568 on Neural Morphological and Statistic Methods*, July 10–11 (San Diego).

Heeger, D. J. 1987. Model for the extraction of image flow. Optical Society of America **4**(8), 1455–1471.

Heikkilä, J. and Silvèn, O. 1997. A four-step camera calibration procedure with implicit image correction. In: *CVPR'97: Proceedings of IEEE Computer Society Conference on Computer Vision and Pattern Recognition* (San Juan, Puerto Rico), pp. 1106–1112.

Hofstee, J. W. 1994. Handling and spreading of fertilizers: Part 3, measurement of particle velocities and directions with ultrasonic transducers, theory, measurement system, and experimental arrangements. Journal of Agricultural Engineering Research **58**(1), 1–16.

Horn, B. K. P. and Schunck, B. 1981. Determining optical flow. Artificial Intelligence **17**, 185–203.

Kardouchi, M., Dipanda, A. and Legrand, L. 1997. Motion estimation with markov random fields using a direct algorithm. SPIE, International Symposium on Optical Applied Science and Engineering, **3101**, Berlin, pp. 95–103.

Olieslagers, R. 1997. Fertilizer distribution modeling for centrifugal spreader design. Ph.D. Thesis (University of Leuven, Belgium).

Orkisz, M. and Clarysse, P. 1996. Estimation du flot optique en présence de discontinuités: une revue (Optical flow estimation preserving discontinuities : A survey). Traitement du Signal, Numéro spécial "Le mouvement dans les signaux et les images" **13**(5), 489–513.

Patent No 0109749. 24 July 2001. Dispositif de mesure du débit massique sur distributeur centrifuge de particules solides (Measurement system of solid particles mass flow on a centrifugal distributor).

Patterson, D. E. and Reece, A. R. 1962. The theory of centrifugal distributor I: Motion on the disc, near-centre feed. Journal of Agricultural Engineering Research **7**(3), 232–234.

Pellerin, D., Spinéi, A. and Guérin-Dugué, A. 1996. Optical flow based on combined gabor filters. Revue Traitement du Signal **13**(1), 13–23.